MRS Spring Meeting, *Proc. Symposium P: Chemical Mechanical Polishing,* San Francisco, CA, Apr. 1999.

PATTERN DEPENDENT MODELING FOR CMP OPTIMIZATION AND CONTROL

D. BONING, B. LEE, C. OJI, D. OUMA, T. PARK, T. SMITH, and T. TUGBAWA
Massachusetts Institute of Technology, Microsystems Technology Laboratories,
EECS, Room 39-567, Cambridge, MA 02139

ABSTRACT

In previous work, we have formalized the notions of “planarization length” and “planarization response function” as key parameters that characterize a given CMP consumable set and process. Once extracted through experiments using carefully designed characterization mask sets, these parameters can be used to predict polish performance in CMP for arbitrary product layouts. The methodology has proven effective at predicting oxide interlevel dielectric planarization results.

In this work, we discuss extensions of layout pattern dependent CMP modeling. These improvements include integrated up and down area polish modeling; this is needed to account for both density dependent effects, and step height limits or step height perturbations on the density model. Second, we discuss applications of the model to process optimization, process control (e.g. feedback compensation of equipment drifts), and shallow trench isolation (STI) polish. Third, we propose a framework for the modeling of pattern dependent effects in copper CMP. The framework includes “removal rate diagrams” which concisely capture dishing height and step height dependencies in dual material polish processes.

I. MOTIVATION: PATTERN DEPENDENT CMP CONCERNS

The motivation for this work is the presence of substantial pattern dependencies in CMP. As illustrated in Fig. 1, these concerns arise in a variety of key CMP process applications. In oxide or interlevel dielectric (ILD) CMP, the global planarity or oxide thickness differences in different regions across the chip is a key concern. In addition, the remaining local step height (or height differences in the oxide over patterned features and between patterned features) may also be of concern, although such local step heights are typically small compared to the global nonplanarity across the chip resulting from pattern density dependent planarization. In shallow trench isolation (STI), one is typically concerned about dishing within oxide features resulting from over-polish, as well as the erosion of supporting nitride and in some cases the details of the corner rounding near active areas. In metal polishing (such as in copper damascene), one is concerned also with dishing into metal lines, as well as the erosion of supporting oxide or dielectric spaces in arrays between lines.

In this paper, we begin by reviewing previous work on characterization and modeling of oxide CMP pattern dependencies. In Section II, we review the density-dependent oxide CMP model, as well as the important determination of “effective density” based upon a planarization length or planarization response function determination. In Section III, we also review a recent advance in oxide modeling, through which a step height dependent model (proposed elsewhere) has been integrated with the effective density model to produce an integrated time-evolution model for improved accuracy in step height and down area polish prediction. In Section IV we present example applications of the oxide characterization and modeling methodology. These include, first, some comments on the importance of such effects in the design and optimization of the CMP process, and second, an example in which pattern dependent models are integrated with a run by

run feedback control scheme to enable pattern dependent oxide control. As a third example, the application of oxide CMP modeling to STI process issues is discussed. In Section V we further generalize the modeling approach to enable application to pattern dependent issues in copper CMP. In particular, we contribute a concise "removal rate diagram" concept that helps to identify the key step height and material dependencies in copper CMP modeling. Finally, a summary is presented in Section VI.

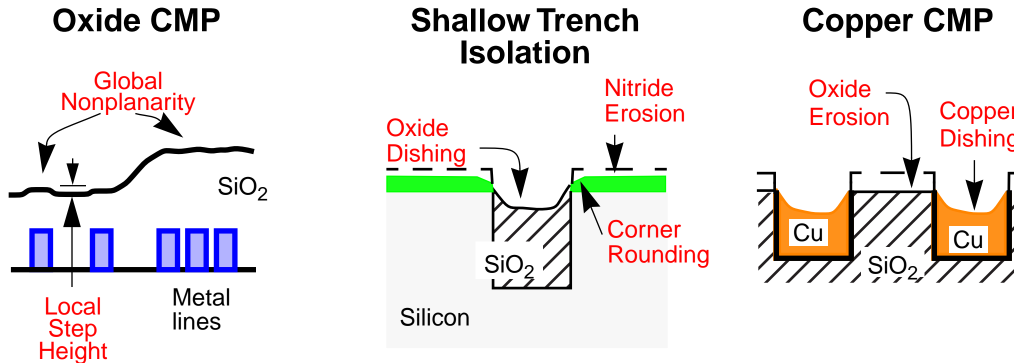

Figure 1. Pattern-dependencies of concern in typical CMP process steps.

II. REVIEW: OXIDE CMP DENSITY DEPENDENT MODELING

In previous work, the fundamental problem we have examined in oxide modeling is the global non-planarity within the die resulting from pattern dependent planarization, as shown in Fig. 2 [1,2]. The goal of our approach has been to achieve efficient chip-level modeling of the oxide thickness across arbitrary product die patterns [3]. The approach has been simplified analytic modeling, in which the removal rate at any location is inversely proportional to the effective density of raised topography. The determination of "effective density" becomes the crucial element in the model: it is through the effective density that the pad and process "sees" that nearby topography influences the polish at any given location.

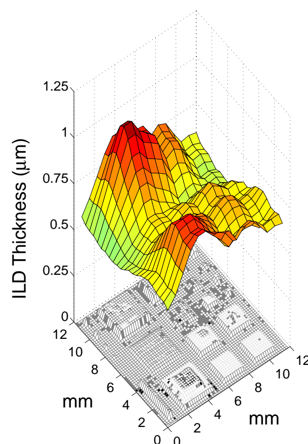

Figure 2. Die-level oxide thickness variation remaining after ILD CMP, resulting from topography arising from pattern dependencies in the underlying metalization.

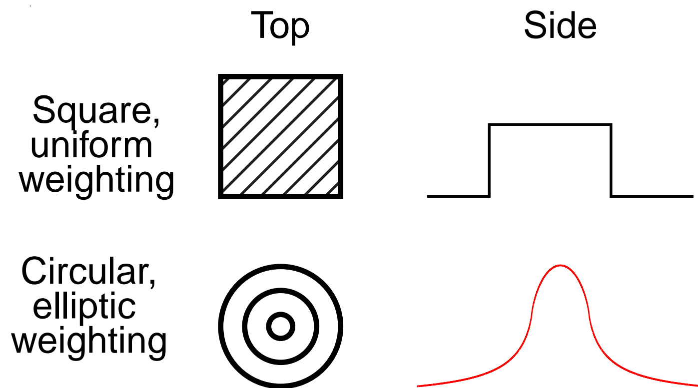

Figure 3. Window shapes and weighting functions used in calculation of effective density from a given layout.

In our early work, square uniformly weighted windows were used to calculate the effective density, as illustrated in Fig. 3. More recently, we have found substantially better modeling can be

achieved with a circularly symmetric, elliptically weighted response function as also shown in Fig. 3 [4]. This response function shape is physically motivated, and corresponds to elastic pad bending or deformation profiles. As part of the methodology for modeling, test chips with "step density" test patterns have been devised to improve the extraction of the planarization response length parameter.The key elements of the density-based model are that the removal rate at any given location depends on the effective density at that location:

$$PR = \frac{K}{\rho(x, y, PL)} \tag{1}$$

where K is the blanket film polish rate, x and y are spatial locations on the die, and ρ is the effective density which depends on the PL or planarization length (size of the weighting window) used to average local densities. The computation of effective density is illustrated in Fig. 4 for the dielectric characterization mask, which contains regions with gradual changes in local block density, regions with large step density changes between blocks, and regions with equal designed density (50%) and varying pitch. The resulting effective density map is directly related to the final oxide thickness over patterned features observed at the completion of oxide CMP, enabling the extraction of the planarization length from such characterization data.

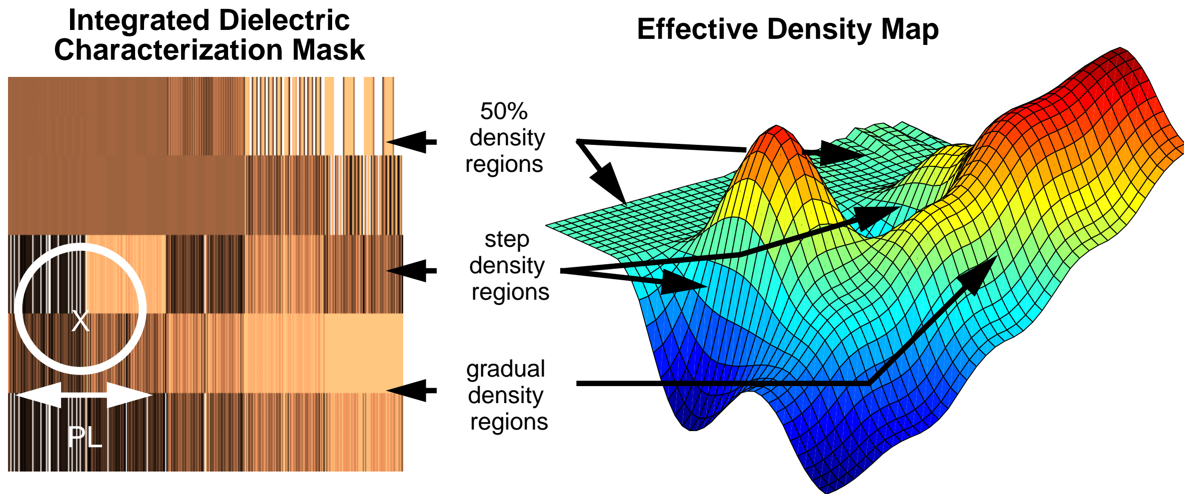

Figure 4. Calculation of effective density for a given layout using the elliptically weighted planarization response function. The characterization mask shown includes structures clearly important in the effective density map [3].

In previous work, details of the planarization response function and its relationship to the pad and process conditions has been discussed [4]. As shown in Fig. 5, the "shape" or weighting of the elliptic response is based on the deformation of elastic material (e.g. the pad) under a spatially localized load of width L. The resulting deformation $w(r)$ can be expressed as:

$$w(r) = \frac{4(1-v^2)qa}{\pi E}\int_0^{\frac{\pi}{2}}\sqrt{1-\frac{r^2}{a^2}\sin^2\theta}\,d\theta \qquad \text{within the load area (r<a)}$$

$$w(r) = \frac{4(1-v^2)qr}{\pi E}\left[\int_0^{\frac{\pi}{2}}\sqrt{1-\frac{a^2}{r^2}\sin^2\theta}\,d\theta - \left(1-\frac{a^2}{r^2}\right)\int_0^{\frac{\pi}{2}}\frac{d\theta}{\sqrt{1-\frac{a^2}{r^2}\sin^2\theta}}\right] \qquad \text{outside load area (r>a)} \tag{2}$$

with E being Young's modulus, ν Poisson's ratio, and q the load. Using this density weighting function, it becomes possible to efficiently calculate the effective density for an entire layout as shown in Fig. 4 using a simple 2D convolution (or equivalently, a Fourier transform and inverse transform manipulation) of the weighting function and local layout density.

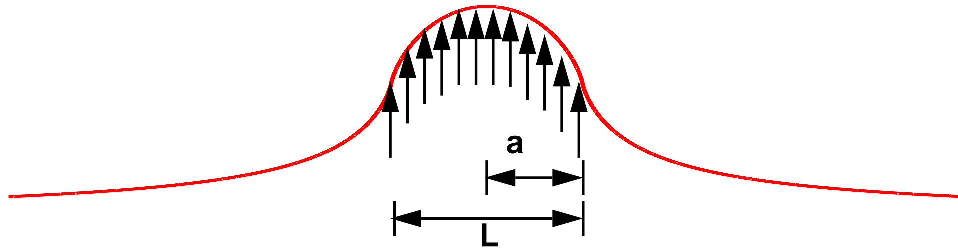

Figure 5. Planarization response function based on elliptic deformation response of an elastic material to a localized load.

Under further simplified assumptions as detailed in [1], excellent fits of the density dependent oxide polish model to experimental data can be achieved. A key assumption in the basic density dependent models is that there exists at all times "planar contact" of the pad on the feature scale: the pad is assumed to only contact the "raised areas" over patterned features and not to contact the "down areas" between features so long as a local step height exists between the up and down areas. Grillaert identified this condition as the "incompressible" pad model [5], and noted that this results in a step height that decreases linearly in time. Using the effective density model and this incompressible assumption, a fit between the model and oxide planarization experiments with surprisingly small error can be achieved. As shown in Fig. 6, for oxide thickness in both raised and down areas remaining after oxide planarization using the mask previously shown in Fig. 4, root mean square errors below 300 Å can be achieved.

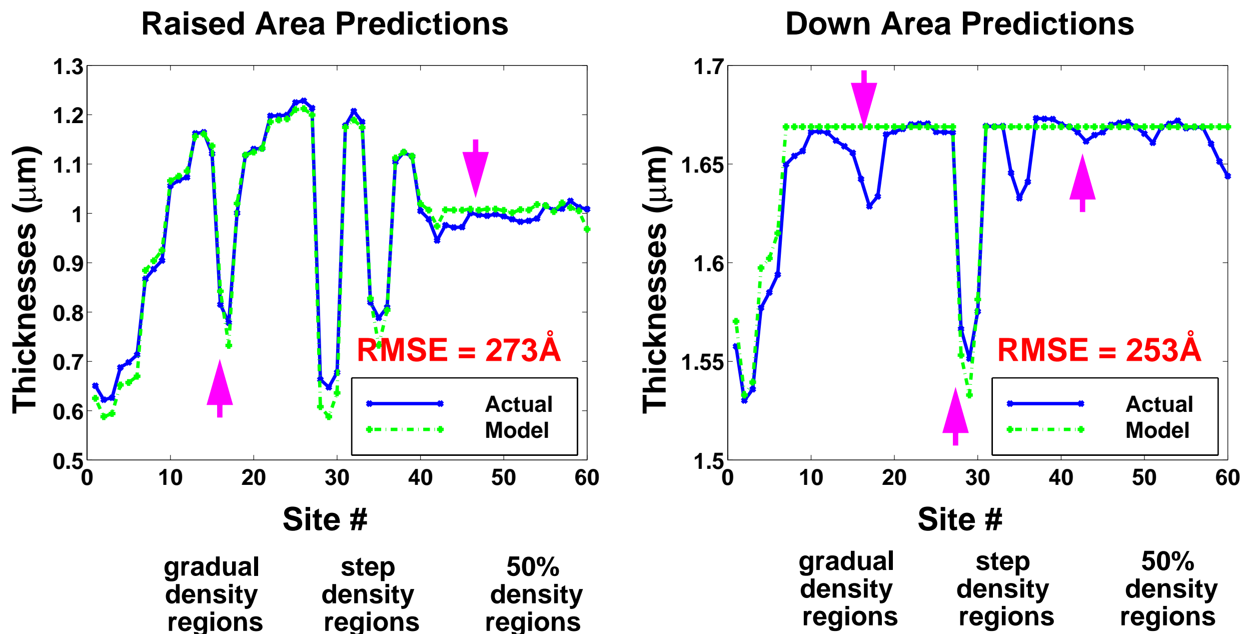

Figure 6. MIT density dependent model applied to both "up" (over metal) and "down" (between metal) oxide thickness resulting from oxide CMP:

III. INTEGRATED MODEL: EFFECTIVE DENSITY AND STEP HEIGHT

An alternative model for the dependence of local step height reduction has been proposed by numerous workers, including Burke [6], and Tseng [7]. In this case, it is proposed that the rate of step height reduction is proportional to the remaining step height. This is based on relative rates of material removal on the up and the down features depending on an allocation of the down pressure between these up and down regions. Under this "compressible pad" model, the step height exponentially decays in time as the local pad pressure differential decreases leading to less effective reduction in time of the smaller and smaller remaining step height. Grillaert et al. [5] proposed a transition model illustrated in Fig. 7 in which large step heights sufficient for the pad to entirely lose contact with the down areas are initially present (during which the planarization proceeds as under the incompressible pad model), and at some transition height h_1 or contact time t_c the pad begins to contact the down areas and the compressible model is then appropriate:

$$h_1 = h_0 - \left(t_c \cdot \frac{K}{\rho}\right) \tag{3}$$

In that work, a density dependence is also indicated and verified but required or assumed use of the designed local density for large array test structures.

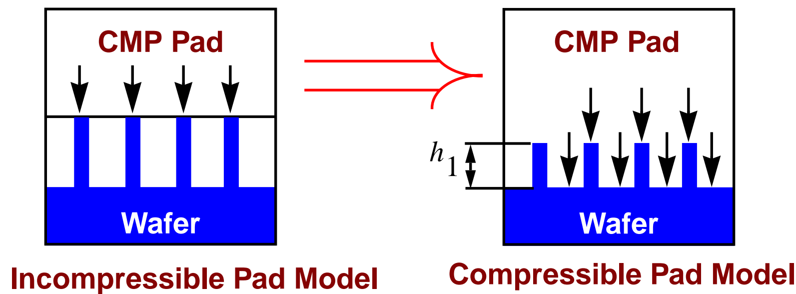

Figure 7. Transition from the incompressible pad model to a compressible pad model as proposed by Grillaert et al. [5]. The transition occurs at some transition height h_1 or contact time t_c.

In examining the regions where substantial errors exist in the simple effective density model of Fig. 6, Smith et al. [8] identified that many of the errors appear to be due to the idealized incompressible pad model. In order to gain the benefits of efficient effective density determination from the MIT model and the benefits of accurate down area and step height determination from the Grillaert et al. model, an integrated approach was proposed. While the original MIT model produced results that depend on two extracted model parameter -- the planarization length (PL) and the blanket removal rate (K) -- the integrated model also extracts the exponential step height decay time constant (τ) and the contact height (h_1) for each site. In the integrated model, the contact height is forced to depend on the effective pattern density as follows:

$$h_1 = a_1 + a_2 \cdot e^{-\rho / a_3} \tag{4}$$

where a_1, a_2, and a_3 are parameters that are also extracted [8]. The extraction or fit is performed as two iterative loops: the outer loop varies the *PL* to calculate effective density, at which point the inner loop performs an optimization to find the best values for the other model coefficients that minimize model error. These loops are iterated to find the best set of the six model parameters which minimize the overall squared error.

The resulting model fit is substantially improved, as illustrated in Fig. 8. In particular, the large errors where the effective density model over-estimated the down area polish have been dramatically reduced. The remaining error is on the order of 100Å as compared to the early RMSE of 273A. With 100Å model error, it becomes possible to contemplate using the model in such activities as feedback control where extreme model accuracy is demanded. On the other hand, some regions (notably the large regions with low density which planarized relatively quickly) with substantial model error are still apparent in Fig. 8. It is conjectured that a large-scale pad bending or flexing limit or effect may be present, such as that recently discussed by Grillaert [9].

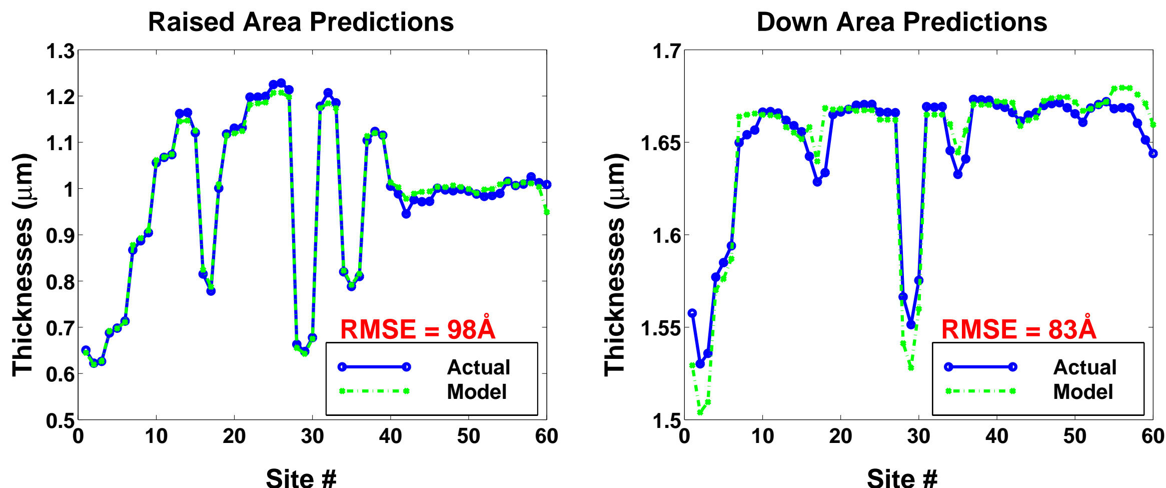

Figure 8. Model predictions and experimental data comparison for the integrated effective density and step height model [8].

IV. CMP APPLICATIONS

In this section, three example applications intimately related to the pattern dependent behavior of CMP are briefly discussed. First, we note the relative importance of die-level effects with respect to typical wafer-scale nonuniformity. Second, we describe recent application of the integrated density and step height model to the run by run control of ILD CMP. Finally, we summarize issues in the application of density models to prediction of shallow trench isolation.

Oxide CMP Process Optimization

The modeling and characterization of pattern dependent variations in oxide CMP further demonstrate the importance of these effects in the design of a viable CMP process. Given the magnitude of the oxide thickness variation present after planarization in comparison to the variation across the wafer as shown in Fig. 9, it is clear that process optimization should be driven by the die-level variation as much as if not more so than by the wafer-level variation.

ILD CMP Run by Run Control

A well-known problem in CMP is that the pad wears over long periods of time as the number of wafers processed on the pad increases. Various strategies have emerged to address this concern, including ex-situ and in-situ pad conditioning, and run by run control. In previous work, we have demonstrated run by run control on blanket wafers, in which polish time and other process parameters are adjusted for the next or later wafer based on measurements on a previous wafer to compensate for removal rate and uniformity degradation [10,11]. In practical use, however, such run

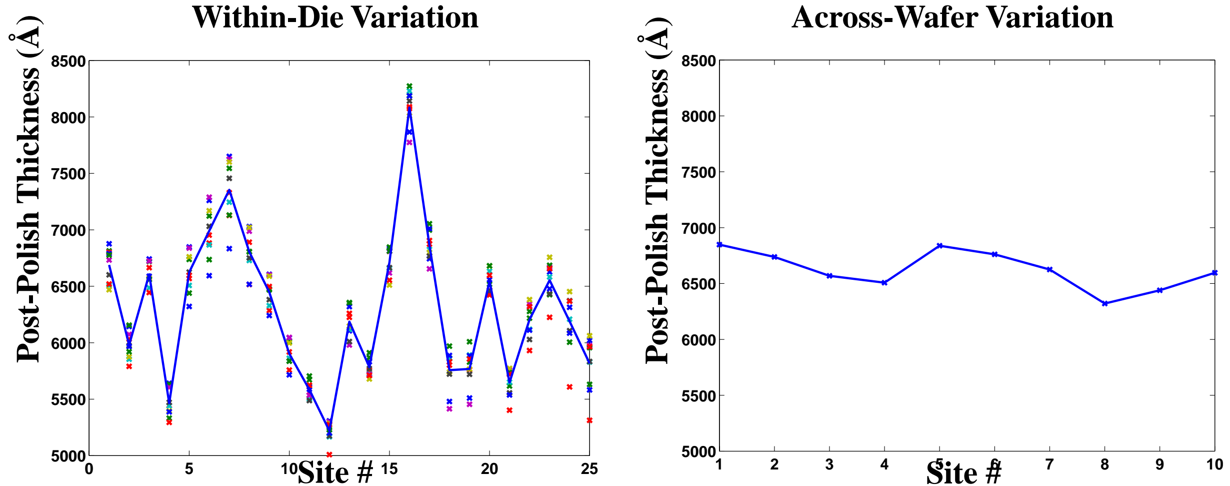

Figure 9. The within-die variation in comparison to across-wafer variation in an ILD CMP process. Shown at left are the thicknesses remaining as a function of 25 site locations within the die; points for five different die across the wafer are indicated. Shown at right is the thickness for the same die position measured at 10 different sites across the wafer.

by run control faces additional barriers to adoption. First, the film thickness measurements have been difficult to acquire on an automated or timely basis. This problem has been largely overcome by the recent availability of the Nova on-line sensor integrated with the CMP tool by which patterned wafer film thickness measurements can be taken on each wafer immediately after polishing [12]. The second barrier to run by run control, however, is the fact that in most fab operations, the same CMP tool and recipe is used across multiple product or product layers. Each product has a unique pattern which, as described above, can have a very large impact on the actual film thicknesses that result within the die on such wafers. As a result, it is typical that retargeting or "look-ahead" wafers are used for each lot of wafers with a different pattern to be processed on the CMP tool.

The ability to accurately model die pattern evolution as discussed in this paper provides a solution applicable to the run by run control of multi-product patterned wafers [13]. As shown in Fig. 10, a feedback control loop incorporating the integrated density and step-height pattern dependent model was developed. For each device type, an appropriate set of model parameters (including effective blanket rate *BR* and planarization length) were determined. The model for the effective "blanket rate" includes a term *Delta(n)* that is updated on each run *n* to track the tool drift in rate over time due to pad and consumable wear:

$$BR(n) = BR(0) + BR_Device(D) + Delta(n) \tag{5}$$

The model update is based on seven measurements on four die taken on each patterned wafer using the on-line Nova sensor. The updated blanket rate is then used in conjunction with the pattern dependent model to select the best time for the next wafer of either product type to achieve the desired average target thickness (estimated values from the pattern dependent model of a four die average of 252 sites). The experimental results for a control experiment across two different patterned wafer types is shown in Fig. 11, where we see that +/- 100Å control around the average target thickness has been achieved.

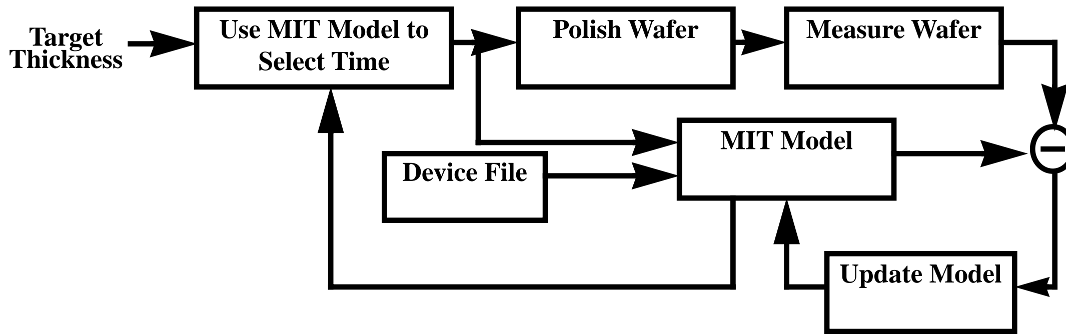

Figure 10. Run by Run controller for CMP using the integrated MIT density/step-height model to predict and control film thicknesses for different product-dependent device files.

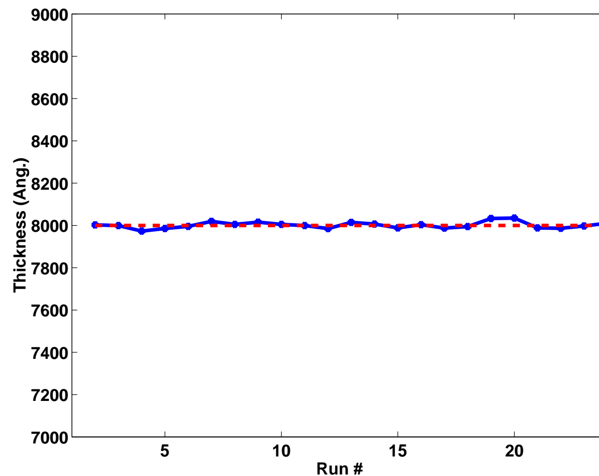

Figure 11. Run by run control over two different pattern wafer types. Wafers were alternated between the two wafer types, with the run by run controller adjusting polish time based on patterned wafer measurements and pattern dependent predictions between each run.

STI Modeling

A third area for application of the effective density and integrated density/step-height models is in the area of shallow trench isolation (STI) formation. As shown in Fig. 1, several pattern dependent concerns arise, including oxide dishing and nitride erosion. In previous work, we have found that good modeling of the oxide overburden stage can be achieved, provided that one takes great care in modeling the effective density resulting from different deposition topographies (e.g. conformal vs. HDP depositions) [14]. We have also found that nitride erosion can be adequately predicted for large active area regions. However, an acceleration of nitride erosion beyond that explain based simply on a density effect is also observed; this issue will be discussed below in the context of copper CMP modeling. Further work to apply the integrated density/step-height model to oxide dishing is also needed.

V. MODEL GENERALIZATION FOR COPPER CMP

To this point we have discussed recent model extensions in the context of oxide CMP. As illustrated schematically in Fig. 1, dishing and erosion concerns in copper damascene processing also

require pattern dependent modeling. In this work, we have taken initial steps toward developing a model framework for copper CMP. In particular, we propose a generalization of the density and step-height integrated model for cases where different materials (in this case copper and oxide) are simultaneously undergoing polish. A new notion of "removal rate diagrams" is proposed that concisely captures removal rate dependencies on step height (either as-deposited/plated, or as created due to dishing). We also note additional issues that we believe the model must incorporate to predict copper polish for both wide and fine-line features.

Stages of Copper Polish

A key requirement for copper planarization and polish modeling is the need to track the removal rate of metal and oxide during each stage of the copper polish. In the case of the typical copper damascene process, three different phases or stages in the polish must be addressed, as illustrated in Fig. 12. In the first stage, only copper removal takes place as the copper overburden is planarized and removed. In the second stage, the barrier or liner material must be removed from field and oxide regions; during this stage, it is likely that some degree of dishing in the copper lines may occur. In the third stage, "over-polish" to ensure clearing of the copper and barrier across the entire die and wafer is performed, during which time substantial dishing and erosion may take place in any given structure. In this paper, we focus only on the first and third stages under the assumption that the second stage is very short; similar approaches can also be used to carefully model the second stage.

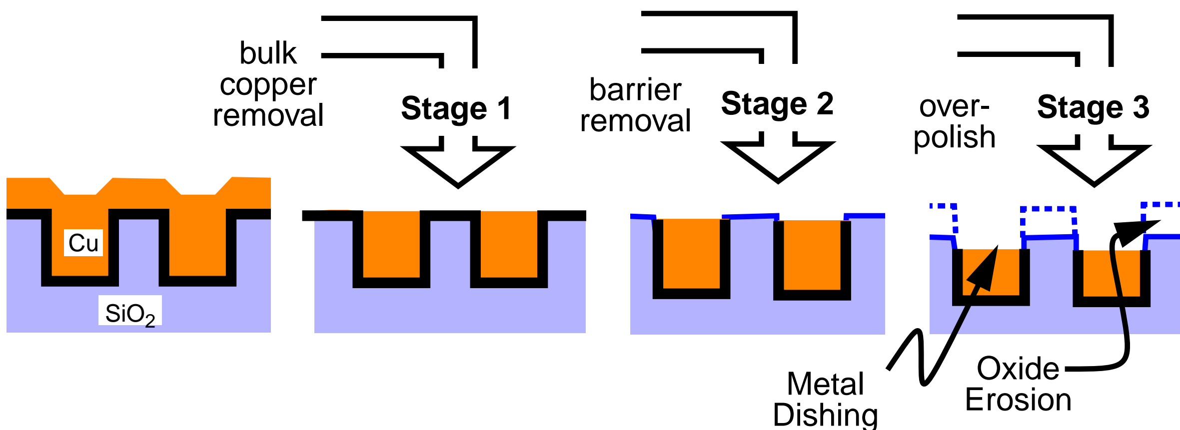

Figure 12. Stages in copper polishing encompassing bulk copper removal, barrier removal, and overpolish creation of dishing and erosion.

"Removal Rate" Diagrams

In the first stage of copper planarization, the integrated density and step-height model described earlier for oxide modeling is again used. A removal rate diagram for this stage is shown at the left of Fig. 13. With time proceeding from the right edge of the local step height (horizontal) axis toward the left, the following occurs. First, a pre-existing step height larger than the "contact" height exists, so that the up copper areas polish at the blanket copper rate modified by the effective pattern density. Note that future work is needed to understand what components or portion of the copper blanket rate are indeed pressure or pattern density dependent; recent work elsewhere on Preston equation modifications [15] are essential to the correct modeling of the impact of density at this and other stages. Continuing in Fig. 13, as time progresses the step height decreases until the contact height h_{ex} is reached; at this point, the copper up area rate decreases linearly with

decreasing step height, while the down region rates increase with decreasing step height. When the step height goes to zero local planarity has been achieved and polish continues in both the "up" and "down" areas at the blanket rate.

In the third or overpolish stage, polish rates of both inlaid copper lines or features and of supporting oxide spaces must be considered as shown in the right side of Fig. 13. At the start of this stage, some small (or ideally zero) dishing height is in effect; as time progresses to the right in Fig. 13 this dishing height increases. In the case of "down area" or copper features, the local polish rate decreases linearly with this dishing height; this would continue until some d_{max} height at which pad contact with the down areas is lost and the rate would then go to zero. In the case of the oxide spaces, on the other hand, the local removal rate increases linearly as the dishing height increases. The removal rate diagram clearly indicates an equilibrium or steady-state point (as noted in the case of tungsten polish by Elbel et al. [16]) where both the copper and oxide rates are equal. This steady-state dishing d_{ss} point is the actual maximum degree of dishing one would observe in a given structure.

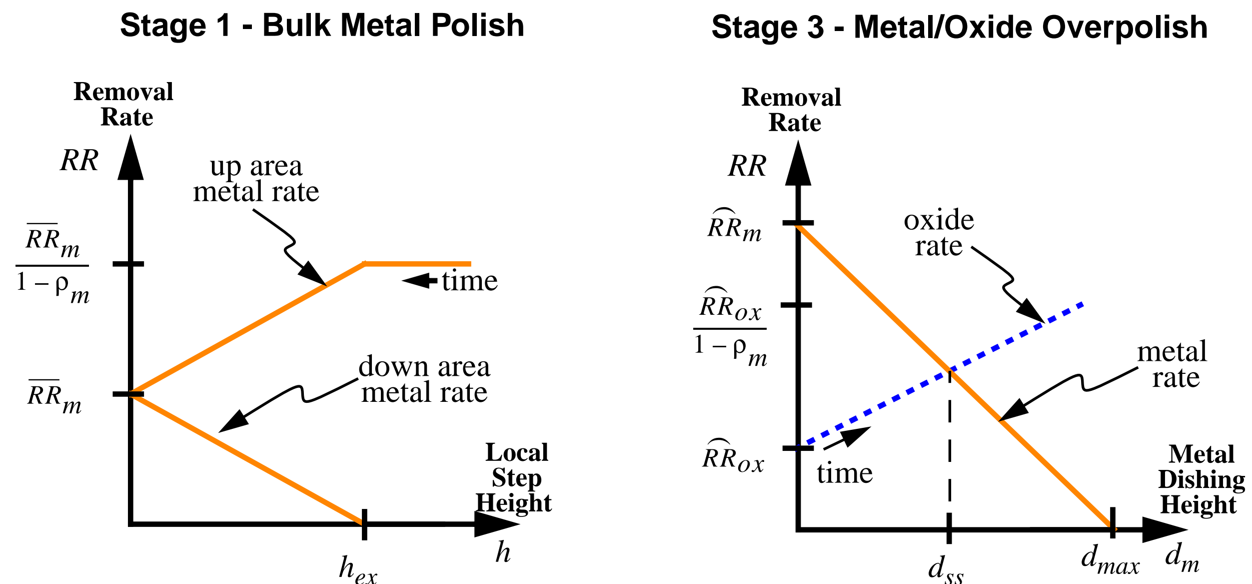

Figure 13. Removal rate diagrams for the bulk metal and overpolish stages in copper CMP. Shown at left is the stage 1 removal rate for the metal up and metal down areas, as a function of the local step height. Shown at right are the stage 2 removal rates for the metal (in trenches) and oxide (spaces) as a function of the dishing height.

Dishing and Oxide Removal Rate Dependencies

The proposed copper model framework described above captures three key effects: step height (or dishing height) dependencies, effective density dependencies, and selectivity between removal in multiple material polish systems. The parameters shown in the removal rate diagrams also need to be extended to account for two additional important pattern dependent effects, as shown in Fig. 14.

First, the d_{max} parameter, which expresses the height at which the pad would lose contact with copper trenches, is also likely to be a pattern dependent parameter. One conjecture is that this parameter may increase as a function of the copper line width, as shown in the left side of Fig. 14.

Alternatively, the d_{max} parameter may be a function of pattern density, as is believed to be the case for contact height in oxide polishing [5,17,8]. More experimental work is needed to identify and characterize this dependency.

A second additional pattern dependent effect needs to be accounted for. As illustrated in the right side of Fig. 14, the effective oxide removal rate (which is modified in the removal rate diagram by the effective density) may also have an oxide space width dependence. That is, the removal rate diagram already accounts for the effective density, but for small oxide space sizes one observes even faster removal of the oxide space than density alone explains. We conjecture a relationship as shown in Fig. 14 based on localized high pressures near the edges of raised features. From contact wear analysis, as the oxide space width becomes small these high pressure peaks extend over a larger portion of the entire oxide feature and accelerate the oxide removal.

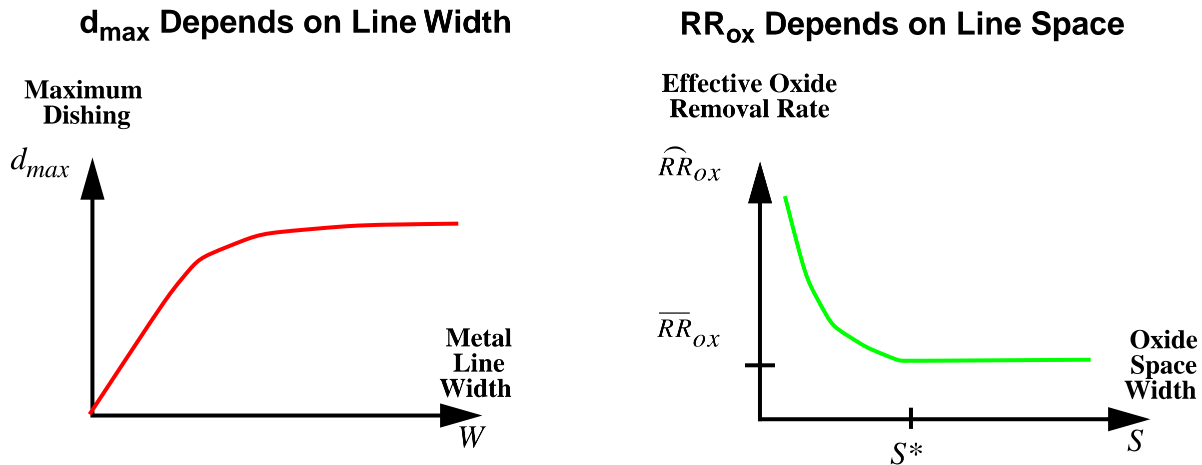

Figure 14. Dishing and oxide erosion rate parameter dependencies. Shown at left is a conjectured dependency between the maximum dishing d_{max} and the metal line width. Shown at right is a schematic acceleration of the oxide removal rate for small oxide space widths.

Copper Model Status: Extraction/Validation of Model

A model framework has been proposed here for prediction of copper polish pattern dependencies. Current work is focused on electrical and physical calibration and validation of model elements. Test masks have been designed which span a variety of pattern parameters, and experimental exploration of process and consumable impact on the polish is in progress [18,19]. The goal is to (a) extract copper model parameters from these experiments, and (b) validate and extend the model as needed for accurate prediction of copper line thickness, copper dishing, and oxide erosion pattern effects. Several challenges need to be addressed. For example, the extraction of planarization length for copper is complicated by the difficulty in making thin film measurements over patterned features in the case of opaque materials such as copper. New approaches, including advanced metrology and alternative mask features may be needed for planarization length and other parameter extraction [20].

VI. SUMMARY AND CONCLUSIONS

In this paper, we have reviewed initial work on oxide planarization modeling encompassing an effective density dependence, and extensions to the model to integrate both effective density and step height dependencies. The integrated model enables efficient full chip oxide thickness predic-

tion with model fits have better than 100Å accuracy achieved. Challenges remain even in oxide modeling, including prediction with especially hard or solo pads, and prediction for alternative slurries and consumable sets.

Several application of oxide models have been presented. These included the importance of within-die characterization and prediction for process optimization, and the use of the pattern dependent model in run by run feedback control. Work has also been done to apply the density model to STI polish. We believe that the generalized framework presented for copper polish is also applicable to the modeling of dishing and erosion in STI CMP.

Finally, we have proposed a model framework for copper CMP simulation. Characterization methods (masks with physical, electrical test structures) for single- and multi-level pattern-dependencies are also under development, and we are pursuing ways to overcome challenges in model parameter extraction and validation.

ACKNOWLEDGMENTS

We would like to acknowledge collaborations and discussions with Dale Hetherington of Sandia National Laboratories; Simon Fang, Greg Shinn and others at Texas Instruments; Tony Pan and others at Applied Materials; Steve Hymes, Konstantin Smekalin and others at SEMATECH; Larry Camilletti at Conexant; and Jung-Hoon Chun, Nannaji Saka, and Jiun-Yu Lai at MIT. This work has been supported in part by DARPA under contact #DABT63-95-C-0088, by the NSF/SRC Engineering Research Center for Environmentally Benign Semiconductor Manufacturing, and by PDF Solutions, Inc.

REFERENCES

1. B. Stine, D. Ouma, R. Divecha, D. Boning, J. Chung, D. Hetherington, I. Ali, G. Shinn, J. Clark O. S. Nakagawa, S.-Y. Oh, "A Closed-Form Analytic Model for ILD Thickness Variation in CMP Processes," *Proc. CMP-MIC Conf.*, Santa Clara, CA, Feb 1997.
2. B. Stine, D. Ouma, R. Divecha, D. Boning, J. Chung, D. Hetherington, C. R. Harwood, O. S. Nakagawa, and S.-Y. Oh, "Rapid Characterization and Modeling of Pattern Dependent Variation in Chemical Mechanical Polishing," *IEEE Trans. on Semi. Manuf.,* vol 11, no. 1 pp. 129-140, Feb 1998.
3. D. Ouma, D. Boning, J. Chung, G. Shinn, L. Olsen, and J. Clark, "An Integrated Characterization and Modeling Methodology for CMP Dielectric Planarization," *International Interconnect Technology Conference*, San Francisco, CA, June 1998.
4. D. Boning, D. Ouma, and J. Chung, "Extraction of Planarization Length and Response Function in Chemical-Mechanical Polishing," *Materials Research Society 1998 Spring Meeting*, San Francisco, CA, May 1998.
5. J. Grillaert, M. Meuris, N. Heylen, K. Devriendt, E. Vrancken, and M. Heyns, "Modelling step height reduction and local removal rates based on pad-substrate interactions," *CMP-MIC*, pp. 79-86, Feb. 1998.
6. P. A. Burke, "Semi-empirical modeling of SiO_2 chemical-mechanical polishing planarization," *Proc. VMIC Conf.,* pp. 379-384, Santa Clara, CA, June 1991.
7. E. Tseng, C. Yi, and H. C. Chen, "A Mechanical Model for DRAM Dielectric Chemical-Mechanical Polishing Process," *CMP-MIC*, pp. 258-265, Santa Clara, CA, Feb. 1997.

8. T. H. Smith, D. Boning, S. J. Fang, G. B. Shinn, and J. A. Stefani, “A CMP Model Combining Density and Time Dependencies,” *Proc. CMP-MIC*, Santa Clara, CA, Feb. 1999.
9. J. Grillaert, M. Meuris, E. Vrancken, K. Devriendt, W. Fyen, and M. Heyns, “Modelling the Influence of Pad Bending on the Planarization Performance During CMP,” *Materials Research Society 1999 Spring Meeting*, San Francisco, CA, April 1999.
10. T. Smith, D. Boning, J. Moyne, A. Hurwitz, and J. Curry, “Compensating for CMP Pad Wear Using Run by Run Feedback Control,” *VLSI Multilevel Interconnect Conference,* pp. 437-440, Santa Clara, CA, June 1996.
11. D. Boning, A. Hurwitz, J. Moyne, W. Moyne, S. Shellman, T. Smith, J. Taylor, and R. Telfeyan, “Run by Run Control of Chemical Mechanical Polishing,” *IEEE Trans. on Components, Packaging, and Manufacturing Technology - Part C*, Vol. 19, No. 1, pp. 307-314, Oct. 1996.
12. T. Smith, S. J. Fang, J. A Stefani, G. B. Shinn, D. S. Boning, and S. W. Butler, “On-line Patterned Wafer Thickness Control of Chemical-Mechanical Polishing,” submitted to *Journal of Vacuum Science and Technology A,* November 1998.
13. T. Smith, S. Fang, J. Stefani, G. Shinn, D. Boning and S. Butler, “Device Independent Process Control of Chemical-Mechanical Polishing,” *Process Control, Diagnostics, and Modeling in Semiconductor Device Manufacturing III*, 195th Electrochemical Society Meeting, Seattle, WA, May 1999.
14. J. T. Pan, D. Ouma, P. Li, D. Boning, F. Redecker, J. Chung, and J. Whitby, “Planarization and Integration of Shallow Trench Isolation,” *VLSI Multilevel Interconnect Conference,* Santa Clara, CA, June 1998.
15. S. Ramarajana and S.V. Babu, “Modified Preston Equation For Metal Polishing: Revisited,” *Materials Research Society 1999 Spring Meeting,* San Francisco, CA, April 1999.
16. N. Elbel, B. Neureither, B. Ebersberger, and P. Lahnor, “Tungsten Chemical Mechanical Polishing,” *J. Electrochem. Soc.*, Vol. 145, No. 5, pp. 1659-1164, May 1998.
17. J. Grillaert, M. Meuris, N. Heylen, K. Devriendt, E. Vrancken, and M. Heyns, “Modelling step height reduction and local removal rates based on pad-substrate interactions,” *Materials Research Society 1998 Spring Meeting*, San Francisco, CA, May 1998.
18. T. Park, T. Tugbawa, J. Yoon, D. Boning, J. Chung, R. Muralidhar, S. Hymes, Y. Gotkis, S. Alamgir, R. Walesa, L. Shumway, G. Wu, F. Zhang, R. Kistler, and J. Hawkins, “Pattern and Process Dependencies in Copper Damascene Chemical Mechanical Polishing Processes,” *VLSI Multilevel Interconnect Conference,* Santa Clara, CA, June 1998.
19. T. Park, T. Tugbawa, D. Boning, J. Chung, S. Hymes, R. Muralidhar, B. Wilks, K. Smekalin, G. Bersuker, “Electrical Characterization of Copper Chemical Mechanical Polishing,” *Proc. CMP-MIC,* Santa Clara, CA, Feb. 1999.
20. S. Hymes, K. Smekalin, T. Brown, H. Yeung, M. Joffe, M. Banet, T. Park, T. Tugbawa, D. Boning, J. Nguyen, T. West, and W. Sands, “Determination of the Planarization Distance for Copper CMP Process,” *Materials Research Society 1999 Spring Meeting*, San Francisco, CA, April 1999.